Citation
Aufort, J. and Raiteri, P. and Gale, J.D. 2022. Computational Insights into Mg2+ Dehydration in the Presence of Carbonate. ACS Earth and Space Chemistry. 6 (3): pp. 733-745.
http://doi.org/10.1021/acsearthspacechem.1c00389

Computational insights into Mg^{2+} dehydration in the presence of carbonate

Julie Aufort,[†,‡] Paolo Raiteri,[*,†] and Julian D Gale[†]

†*Curtin Institute for Computation/The Institute for Geoscience Research (TIGeR), School of Molecular and Life Sciences, Curtin University, PO Box U1987, Perth, WA 6845, Australia*

‡*Géosciences Environment Toulouse (GET), Observatoire Midi-Pyrénées, Université de Toulouse, CNRS, IRD, CNES, UPS, 14 Avenue Edouard Belin, Toulouse 31400, France*

E-mail: p.raiteri@curtin.edu.au

Abstract

Water exchange around a free magnesium ion and magnesium paired with carbonate in aqueous solution was studied using free energy methods. Both a rigid-ion and a polarizable force field based on the AMOEBA model were examined. The parameters were adjusted to accurately reproduce the hydration structures of magnesium and carbonate in aqueous solution. The magnesium carbonate ion pairing free energies calculated with both force fields were found to be in excellent agreement with experimental data. Metadynamics simulations of the water exchange conducted with both models revealed that the formation of a contact magnesium carbonate ion pair either decreased the energy barrier for water exchange relative to the free magnesium ion in solution and/or significantly destabilized the magnesium-water contact state. This finding suggests that the presence of carbonate could accelerate the water exchange around magnesium and constitutes a first step towards a better understanding of the atomic-scale mechanisms involved in the nucleation of magnesium-bearing carbonate minerals.

Introduction

The kinetics and thermodynamics of water exchange around magnesium in aqueous solution play a fundamental part in numerous molecular-level mechanisms relevant to both biological and geochemical contexts. Indeed, magnesium ions are ubiquitous in biological systems and play a crucial role in a wide range of major biophysical processes, such as the folding mechanisms of ribonucleic acid (RNA) systems,[1] or the synthesis of ATP from ADP.[2] From a simple ion pairing event, to the transport of Mg^{2+} across cell membranes and its catalytic activity in metalloenzymes, water exchange between the first and second solvation shells of magnesium is the most fundamental step governing all stages of these processes occurring in aqueous environments.[3] In the geological record, dolomite, $CaMg(CO_3)_2$, is the most common carbonate mineral precipitated from seawater, particularly in Palaeozoic and Precambrian sedimentary rocks where hundreds of meters-thick massive dolomite successions are often found.[4] However, dolomite rarely forms in modern environmental systems despite seemingly similar geochemical conditions to past sedimentary cycles and is only scarcely found in highly alkaline and hypersaline environments in which microbial processes are likely to be involved.[5,6] This paradoxical observation and consequential difficulty to understand how past dolomites were formed gave rise to the so-called "dolomite problem"[7] that geochemists are still trying to resolve to this day, particularly as it questions the validity of dolomites as archives of past surface environments (see e.g. Ref 8). The well-established difficulty of synthesizing inorganic dolomite directly from solution under Earth surface conditions, i.e. T<60°C,[9] has long been attributed to kinetic constraints resulting from the strong hydration effects around the magnesium ion.[10]

Dolomite can be successfully synthesized at higher temperatures and such experiments have shown that, under these conditions, formation of disordered high magnesium calcite always precedes the nucleation of dolomite.[11–13] Determining the time scale required for the crystallization of the final well-ordered and stoichiometric dolomite in nature, which has been shown to occur within days via Ostwald ripening at high temperatures,[9] remains

an open question with significant palaeoenvironmental implications regarding the record of early oceanic conditions. A time scale of millions of years for dolomite formation has been suggested, both from dolomitization rates obtained in high temperature experiments (150-220°C) and extrapolated to ambient temperature,[14] and from XRD-based quantification of the cation order of dolomites formed in the last 800 Myr.[15] Aside from elevated temperatures, the rates of dolomitization can also be enhanced by microbial activity, although the ways in which microbial mediation may have contributed to the synthesis of past dolomites under ambient conditions remain under debate. While multiple studies have reported microbially-catalyzed synthesis of dolomite at low temperatures (see e.g. Refs 16,17) it has also been argued that these laboratory culture experiments formed disordered high magnesium calcite without its recrystallization into ordered dolomite.[13,18] Direct early diagenetic formation of dolomite had mostly been restricted to modern dolomites formed in alkaline and hypersaline lakes with high microbial activity. However, recently Chang et al.[8] provided clumped isotope-based evidence of the organogenic and low-temperature origin of late Precambrian dolomites. Despite numerous valuable contributions to solving the dolomite problem since its first mention over a century ago, gray areas in our understanding of dolomite formation persist, particularly due to a lack of atomic-scale knowledge of the mechanisms involved in both inorganic and organogenic pathways.

Computer simulations can provide quantitative data and help gain insight into the thermodynamic and kinetic feasibility of certain molecular-level mechanisms. The first challenge is that the time scale for the exchange of strongly bound water molecules around Mg^{2+}, $\approx$1.5 ms according to ^{17}O NMR data,[19] appears out of reach for most conventional *ab initio* and classical molecular dynamics simulations that typically span tens of ps to hundreds of ns. Therefore, the exploration of any dynamic process around Mg^{2+} in solution requires the use of more advanced computational techniques, such as enhanced sampling methods (e.g. metadynamics, umbrella sampling) to reliably describe and overcome the barrier height for water exchange. For instance, Raiteri et al.[20] did not observe any water exchange in a 50 ns

unbiased classical molecular dynamics simulation of the magnesium ion in water. Schwierz[3] found, using transition path sampling, that a concerted motion of two water molecules and a collective rearrangement of all the water molecules in the first solvation shell of Mg^{2+} was required for water exchange to occur, leading to a much longer time scale than previously estimated, of ≈40 ms. As a result, Grotz et al.[21] developed two sets of force field parameters with formal charges, one of which reproduces the experimental water exchange rate, while the other produces accelerated water exchange dynamics for ion binding observation. However, a second difficulty lies with the magnesium ion's tendency to strongly polarize its environment,[22] a feature that fixed charge rigid-ion force fields fail to consider explicitly. Martinek et al.[23] showed that the use of a full ionic charge force field could lead to an overestimation of the stability of the contact ion pair between divalent cations and negatively charged residues. An improved description can be obtained by taking into account electronic polarization in a mean-field approach called the Electronic Continuum Correction (ECC), which Duboue-Dijon et al.[24] have applied to build a scaled-charge force field for aqueous magnesium. Alternatively, polarizability can be explicitly considered via a model such as AMOEBA that includes both static and self-consistent induced dipoles.[25] We have recently introduced a new set of parameters based on the AMOEBA model for the interaction of calcium in solution with carbonate[26] that have improved the Ca-carbonate ion binding free energies compared to previous non-polarizable models. Finally, while several studies have investigated the dynamics of water exchange around isolated Mg^{2+} in solution, few works have examined the effect of ion pairing on the energy barrier for Mg dehydration. Yang et al.[27] conducted *ab initio* Reaction Path Ensemble (RPE) simulations to explore the possibility that HS^-, a product of bacterial sulphate reduction, might promote Mg^{2+} dehydration in aqueous solution, but found that it had little effect on lowering the water exchange energy barrier. Hamm et al.[28] found, using umbrella sampling, that the solvation sphere of magnesium was unaffected by the presence of aspartate, which did not seem to lower the energetic cost for dehydration, though they used the non-polarizable CHARMM22 force field

for proteins. De Oliveira et al.[29] used a scaled-charge force field to probe the interaction between divalent cations and carboxylate groups, and reported Mg-acetate binding energies but did not investigate the effect of complexation on the water exchange rate. An accurate description of the Mg-carbonate ion pair in solution and quantitative data on the energy barrier for the dehydration of Mg^{2+} in the presence of carbonate remain lacking, despite being an essential first step to the mechanistic understanding of Mg-bearing carbonate mineral formation at the atomic scale.

Here we introduce new parameters for a polarizable model for Mg^{2+} in solution and determine the stability of the magnesium-carbonate ion pair. The influence of including polarization is examined by comparing to results from a new improved parameterization of the rigid-ion model determined here. We find that both models accurately reproduce the experimental data for magnesium-carbonate binding and as a further means of validation we compare to results from *ab initio* molecular dynamics for the case of the contact ion pair. Finally, we assess the influence of carbonate ion pairing on the energy barrier for the dehydration of Mg^{2+} compared to the isolated ion in solution and discuss the possible implications for biomineralization and in a geochemical context.

Methods

All classical molecular dynamics (MD) simulations carried out with the AMOEBA force field, other than for the hydration free energy calculations, were performed using the OpenMM code[30] and run on GPUs using mixed precision[31,32] Additionally, two rigid-ion force fields were used for comparison; the original model developed by Raiteri et al.[20] for magnesium and carbonate ions in solution and a new improved model for Mg and carbonate developed in this work, both combined with the flexible simple point charge water model (SPC/Fw) by Wu et al.[33] All simulations that used the rigid-ion force field developed in this work were run with the same settings used for the AMOEBA simulations. The hydration free energies of the ions

were computed with the free energy perturbation (FEP) package in LAMMPS[34] and an in-house implementation of the BAR method. Both OpenMM and LAMMPS were augmented with the inclusion of the PLUMED plug-in for the metadynamics calculations.[35,36]

Simulations with the AMOEBA force field

We have used the AMOEBA03 model for water[37] and the parameters for water-carbonate interactions were those recently developed by Raiteri et al.[26] In accordance with the standard AMOEBA force field scheme, the mixed van der Waals interaction parameters were obtained using the HGG combination rules. The AMOEBA force field parameters for aqueous Mg^{2+} (q = +2.0, σ = 2.76Å, ε = 1.2552 kJ/mol) were parametrized to reproduce the experimental hydration free energy of the aqueous ion.[38] The computed value of this quantity was determined using the free energy perturbation (FEP) and Bennett acceptance ratio (BAR) methods[39,40] as implemented in TinkerHP.[41] The ion was placed in a water box with a side length of approximately 25 Å and the hydration free energy was computed by scaling the solute charges and solute-solvent interactions using 11 stages each. The scaling λ parameter was set to [0.0, 0.1, 0.2, 0.3, 0.4, 0.5, 0.6, 0.7, 0.8, 0.9, 1.0] for the electrostatic interactions and to [0.0, 0.2, 0.4, 0.5, 0.6, 0.65, 0.7, 0.75, 0.8, 0.9, 1.0] for the van der Waals interactions. Each simulation was run for approximately 0.5 ns at 300 K with a 1 fs timestep. The temperature was controlled using the Andersen thermostat and the water molecules were fully flexible. The interaction cutoff was set to 9 Å while the long-range electrostatic contribution was computed with the particle mesh Ewald method with an accuracy of 10^{-5}. The same threshold was used for the convergence of the calculation of the self-consistent induced dipoles. The AMOEBA interaction between Mg^{2+} and CO_3^{2-} was also supplemented with a Buckingham potential (A = 1750 eV, ρ = 0.3 Å) between magnesium and carbon fitted in order to reproduce the experimental solubility of magnesite. This was achieved by comparing the free energy of magnesite as computed from lattice dynamics, performed using a modified version of the GULP code,[42] with that of the hydrated ions. For this process,

the zero point energy contribution was neglected, as was vibrational quantization, in order to achieve consistency with the application to molecular dynamics.

Simulations with the rigid-ion force field

Despite the careful parameterization of the ions' solvation free energies and of the solubilities of magnesite and dolomite, the $Mg-CO_3$ pairing free energy of the rigid-ion force field computed by Raiteri et al.[20] was almost twice as strong as the reported experimental values. Hence, for this work we have developed a new force field with improved properties. Analogously to the AMOEBA potential, we targeted the experimental hydration free energy of the aqueous ions reported by Marcus,[38] and we used the *ab initio* carbonate water radial distribution functions[26] to guide the refitting of the CO_3-water interactions. In particular, the carbonate C-O bond became more polar, and a new carbon-water repulsive term has been added. The revised force field parameters are reported in Table 1, where they are compared to our earlier parameter set. It is important to note here that for the rigid-ion force field we did not use any combination rules, and any pairwise interactions that are not listed in Table 1 are implicitly zero.

Due to the reduced cost of the FEP calculations with rigid-ion model, the electrostatic and van der Waals interactions were individually scaled using 20 equally spaced λ values and each simulation was 1 ns long. The canonical sampling through velocity rescaling (CSVR) thermostat was used to control the temperature.[43] The PLUMED plug-in was also used for metadynamics calculations.[35]

$MgCO_3$ pairing free energy and dehydration of Mg^{2+}

The $MgCO_3$ ion pairing free energy and the water exchange around both aqueous Mg^{2+} and Mg^{2+} paired with CO_3^{2-} were studied using well-tempered[44] multiple walker[45] metadynamics.[46] For these simulations we used a simulation box of approximately $50 \times 50 \times 50$ Å^3 containing the Mg^{2+} and CO_3^{2-} ions, and 4,182 water molecules. Two collective variables

Table 1: Force field parameters for the rigid-ion model of Raiteri et al.[20] and those developed in this work. The Mg-water interactions are described with a standard Lennard-Jones potential (σ is the distance of zero energy), while the carbonate-water interactions are described with a purely repulsive Buckingham potential, $A\exp(-r/\rho)$.

		Raiteri et al. (20)	This work
Charges (e)	Mg	+2	+2
	C_c	1.123285	1.423285
	O_c	-1.041095	-1.141095
Mg-O_w	ε (eV)	0.001137	0.001137
	σ (Å)	2.82	2.72
Oc-O_w	A (eV)	12534.455133	12534.455133
	ρ (Å)	0.202	0.202
Oc-H_w	A (eV)	340	340
	ρ (Å)	0.217	0.217
Cc-O_w	A (eV)	0.0	12534.455133
	ρ (Å)	–	0.280
Mg-O_c	A (eV)	3944.8613	542.31524
	ρ (Å)	0.238160	0.321740

were used to calculate the $MgCO_3$ pairing free energy; the distance between magnesium and carbon, and the water coordination number around magnesium. The latter was described using the switching function;

$$CN = \sum_i \frac{1-[(d_i-d_0)/r_0]^n}{1-[(d_i-d_0)/r_0]^m} \tag{1}$$

where d_i is the distance between magnesium and the oxygen of the ith water molecule. The parameters were chosen such that the function would overlap with the first peak of the pair distribution function with the water oxygen, leading to values of $d_0 = 1.5$ Å, $r_0 = 1.4$ Å, $n = 6$ and $m = 16$ for the AMOEBA force field. A 1 eV/Å^2 harmonic wall restraining the carbonate group to stay within 16 Å of Mg^{2+} was used to limit the space explored. In order to study how the presence of CO_3^{2-} affects the water exchange around the Mg^{2+} ion, we performed two metadynamics simulations where we used the distance between Mg^{2+} and one specific water molecule and the Mg coordination number with all the other water molecule as CVs. In the first simulation Mg^{2+} was alone in the simulation cell while in

the second it was forced to remain in the contact ion pair state by employing a harmonic restraint at 3.7 Å with a spring constant of 1 eV/Å^2. A further harmonic restraining wall (k = 1 eV/Å^2) on the Mg-water distance CV was also used to limit the space explored to 10 Å. All the AMOEBA metadynamics simulations were run using 16 independent walkers with a bias factor of 15 for an aggregate simulation time of at least 300 ns to ensure well-converged sampling. Gaussians were laid every 1 ps with an initial height of k_BT and width of 0.1 Å for the distance CVs and 0.1 for the coordination number CV.

An identical set of simulations was performed with the rigid-ion force field. Because of the lower computational cost, this allowed for the simulations to be run with 30 independent walkers, which resulted in almost twice as many Gaussians being laid. Due to the higher energy barrier observed with the rigid-ion force field, for these simulations we used a bias factor of 20 to ensure that a correct description of the transition state was achieved. As a further check of the reliability of the results we also repeated the simulations with a bias factor of 30, and no significant difference was observed. All other parameters were kept the same, apart from the switching function that was changed to reflect the differences in the RDF, leading to values of $d_0 = 1.9$ Å, $r_0 = 1.2$ Å, $n = 4$ and $m = 12$ for the rigid-ion force field.

Analogously to our previous work,[47,48] in order to compare the simulation results with experiment we computed the ion pairing free energy from the dissociation constant

$$\Delta G_{IP} = +k_BT \ln\ K_{diss}, \tag{2}$$

which can be obtained by integrating the 1D free energy profile as a function of the ions' separation that we computed using metadynamics simulations, $\Delta G_{meta}(r)$, after it was properly aligned to the analytic solution for the pairing free energy of two point particles interacting

via a screened electrostatic potential,

$$K_{diss} = c_{MD} \int_{R_0}^{R_1} \exp\Big[- w(r)/k_B T\Big] \; 4\pi r^2 \; \mathrm{d}r \tag{3}$$

where c_{MD} is standard concentration in the simulation units, e.g. $6.022{\times}10^{-4}$ atoms/Å^3 and $w(r) = \Delta G_{meta}(r) + k_B T \ln(4\pi r^2)$. The upper limit of the integral, R_1, was set to the limit of the bound state, which was defined as the Bjerrum length ($\approx$ 14Å) for the Mg$-$CO$_3$ pairing free energy and to the maximum of location of the first barrier for water exchange ($\approx$ 3Å). Due to the rapid increase of the free energy at short distance, the lower limit of the integral, R_0, has no bearing on the final result and was set to 2 Å. A complete derivation and numerical validation of these equations can be found in the Supporting Information.

The 1D free energy profile can be easily obtained from the 2D free energy by using the standard statistical mechanical equation

$$\Delta G(s_1) = -k_B T \ln \int \mathrm{d}s_2 \; \exp\Big[- \Delta G(s_1, s_2)/k_B T\Big]. \tag{4}$$

where s_1 and s_2 are the two CVs used in the metadynamics simulations. It is worth mentioning here that an important consequence of this dimensionality reduction is that any free energy barrier measured on a 1D free energy curve will always be lower than or equal to the one measured on the 2D free energy (Figures S7 and S8 in the Supporting Information). This problem is intrinsic to any enhanced sampling method that requires the choice of a set of collective variables to describe the process of interest, and it underscores the importance of identifying all slow degrees of freedom if one is interested in accurately determining the free energy barrier for a rare event.

In addition to the classical simulations, *ab initio* Molecular Dynamics (AIMD), combined with multiple walker metadynamics, was also used to investigate the relative stabilities of the mono and bidentate states of the contact MgCO$_3$ ion pair. Here a cubic box of length 14.784 Å was used containing one ion pair plus 104 water molecules. Calculations were

performed at the BLYP-D3(BJ)/TZ2P level of theory with an auxiliary basis set cut-off of 400 Ry within the Gaussian-Augmented Planewave approach,[49] as implemented in the code CP2K.[50] The initial configurations were generated from the classical force field and then re-equilibrated at 330 K. Note that the higher temperature was used to off-set the systematic over-structuring of water for this level of theory, as suggested by Bankura et al.[51] Well-tempered metadynamics was performed with initial height of 2.5 kJ/mol, width of 0.25 and ΔT of 1000 K. In this case, the two collective variables were the carbonate and water coordination numbers by magnesium. The simulation was run for a cumulative time of 45 ps using two independent walkers, with the following parameters for the switching functions: Mg-O_w $d_0 = 0$ Å, $r_0 = 3.2$ Å, $n = 12$, $m = 24$; Mg-O_c d_0= 0 Å, r_0 =2.8 Å, $n = 16$, $m = 32$, where O_w and O_c indicate the water and carbonate oxygen atoms, respectively.

Results and discussion

Results for the hydration structure of the magnesium cation in water, as computed with the AMOEBA and rigid-ion force fields developed in this work are given in Figure 1. The position of the first peak of the magnesium-oxygen pair distribution function for the AMOEBA model, 2.08 Å, falls within the 2.00–2.15 Å range of experimental values reported for Mg^{2+} in the literature.[52] In comparison, both the current and former non-polarizable rigid-ion force fields predict slightly shorter Mg-O distances in the first solvation shell, with $r_{Mg-O} = 1.94$ Å (this work) and $r_{Mg-O} = 1.99$ Å.[20] This is due to the lack of polarization in the SPC/Fw water model that leads to the underestimation of the water dipole moment adjacent to magnesium and cause the water-cation distances to be shorter in order to reproduce the experimental hydration free energy. However, it should be noted that both the polarizable and rigid-ion parameters developed in this work were fitted to reproduce the hydration free energy values of Marcus,[38,53,54] whereas the previous parameterization of the rigid-ion force field was originally performed to reproduce that of David et al.[55] Compared to the later, the

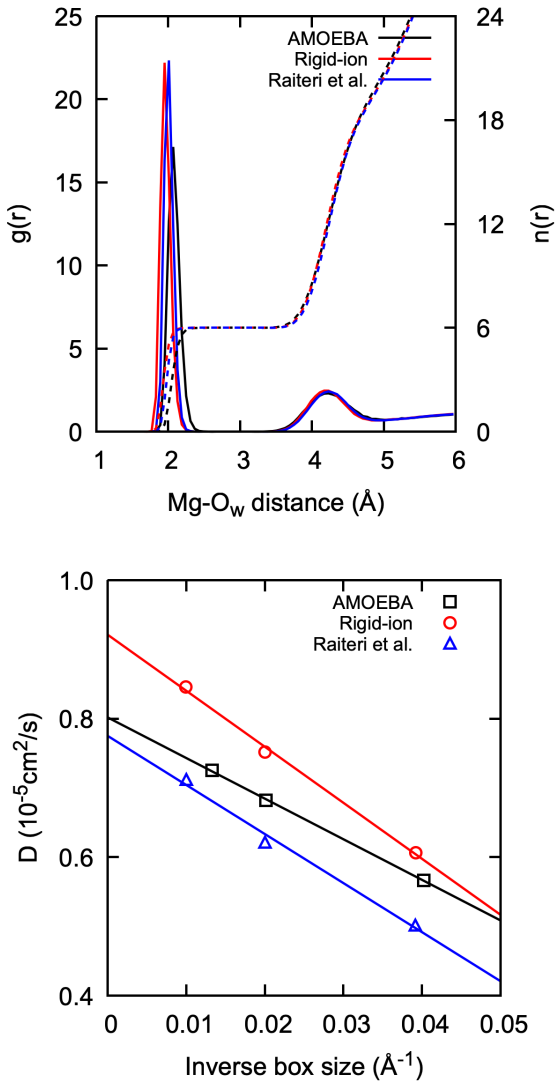

Figure 1: Radial distribution function (solid line, left axis) and cumulative coordination number (dashed line, right axis) of water around Mg^{2+} (top). Self-diffusion coefficient of Mg^{2+} as a function of the simulation box size (bottom).

works of Marcus suggest a more exergonic value of the hydration free energy of magnesium by about 60 kJ/mol. It is worth mentioning here that there is no absolute consensus for the experimental hydration free energy of Mg^{2+} (Table 2), which stems either from the use of different reference values for the hydration enthalpy of the proton,[56] and/or different thermodynamic models.[55]

Table 2: Comparison of the experimental and calculated hydration free energies and self-diffusion coefficients of Mg^{2+} in aqueous solution at 300 K.

	Rigid-ion Raiteri et al.[a]	Rigid-ion this work	AMOEBA	Experiment
$\Delta G_{hydration}$ (kJ/mol)	-1766	-1826	-1826	-1768[b] -1820[c] -1828[d] -1830[e] -1837[f] -1900[g] -1906[h] -1959[i]
D^{∞} (10^{-5} cm^2/s)	0.86	0.92	0.80	0.71[j]

[a]Ref. 20, [b]Ref. 55, [c]Ref. 56, [d]Ref. 54, [e]Ref. 53, [f]Ref. 38, [g]Ref. 57 [h]Ref. 58 [i]Ref. 59 [j]Ref. 60

Earlier works from Noyes et al.[57] and Rosseinsky et al.[58] reported even more exergonic values for $\Delta G_{hydration}$ (Mg^{2+}), -1900 and -1906 kJ/mol, respectively. Recently, Jiang et al.[59] proposed a revised hydration free energy of -1959 kJ/mol that uses Tissandier's proton hydration free energy[61] and a correction for the 1 M standard state that goes in the opposite direction to that of Marcus.[54] However, Marcus[38] has argued against using more negative values of $\Delta G_{hydration}$ (H^+), such as Tissandier's, on the basis that they are incompatible with the electrode potentials measured by Gomer and Tyson.[62] Ultimately, the values of Marcus[38,53,54] fall in the middle of the currently available range of experimental data in the literature, and so they were chosen as the target for the parameterization of both our polarizable model and the new rigid-ion force field.

For all models considered here, the cation remained six-fold coordinated with water throughout the whole length of the unbiased simulations, a known feature of Mg^{2+} compared

to other divalent cations such as Ca^{2+} for which multiple configurations are energetically accessible at room temperature, leading to a variable coordination number.[20,52] No water exchange was observed during the whole MD simulation, suggesting a water residence time greater than 50 ns and a high energy barrier for water exchange at Mg^{2+}, in agreement with previous experimental[19] and theoretical[20,63] results.

The self-diffusion coefficient of magnesium was calculated with three different box sizes (25, 50 and 75 Å) and extrapolated to infinite size to remove finite size effects, as recommended by Yeh and Hummer[64] for accurate comparison between simulations with periodic boundary conditions and experimental measurements. The AMOEBA model was found to overestimate the self-diffusion coefficient by 13% compared to the experimental value but still gave better agreement than the new and former rigid-ion force fields for which the overestimation was about 30% and 21%, respectively.

The water structure around carbonate obtained for the AMOEBA model and rigid-ion force fields is shown in Figure 2 in the form of radial distribution functions (RDF) and 3D atomic density maps and compared to data from *ab initio* MD. Considering that the *ab initio* RDFs between carbonate and water were used to guide the fitting procedure, it is not surprising that both the AMOEBA and new rigid-ion final parameters reproduce accurately the AIMD positions of the first peak of the C-O_w, O_c-O_w and O_c-H_w RDFs, i.e. r_{C-O_w} = 3.5 Å, $r_{O_c-O_w}$ = 2.7 Å and $r_{O_c-H_w}$ = 1.7 Å, respectively. In contrast, the RDF between carbon of carbonate and oxygen of water obtained with the former rigid-ion parameters[20] displays a bimodal first peak, indicating a wider distribution of C-O_w distances in the first hydration shell. This significant difference is also visible in the 3D atomic density maps of water oxygen around carbonate. The AIMD calculations reveal that the water oxygen density in the first hydration shell of carbonate is distributed in three narrow toroids located on top of the carbonate oxygen atoms and centered around the three C-O_c directions. While the AMOEBA and new rigid-ion force fields are both able to reproduce this specific structure, this is not the case of the former rigid-ion parameters[20] which seem to concentrate the

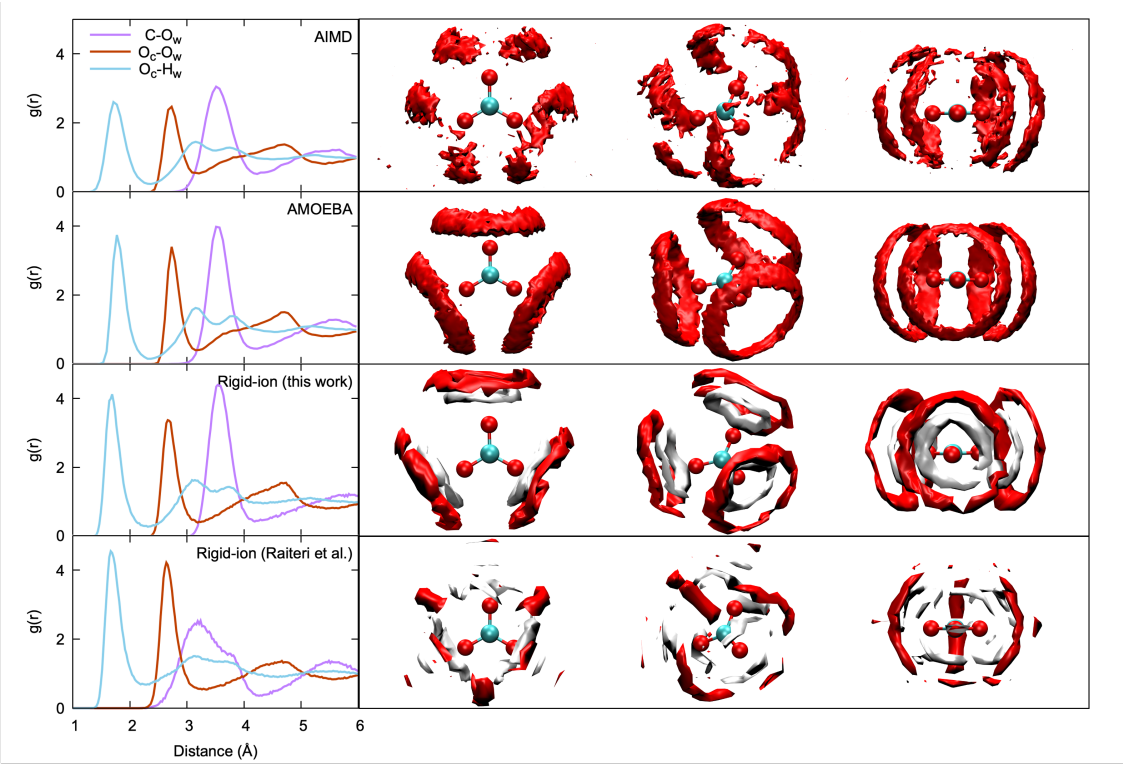

Figure 2: Radial pair distribution functions between carbonate and water (left) and 3D isodensity surfaces of the water structure around carbonate (right) computed using the rigid-ion force field from Raiteri et al.[20] and the new parameterization developed in this work, the polarizable AMOEBA force field from Raiteri et al.[26] and AIMD calculations. The carbon and oxygen atoms are depicted in cyan and red, respectively, while the O_w and H_w atomic densities are shown in red and white, also respectively. A top, tilted and side view is shown for each force field and theoretical method.

water oxygen density predominantly along each C-O_c direction instead. It is worth noting that the new rigid-ion model appears to have a significantly worse hydration free energy that the older force field (Table 3). Extensive attempts to improve this, while maintaining

Table 3: Comparison of the experimental and calculated hydration free energy and self-diffusion coefficient of carbonate in aqueous solution at 300 K.

	Rigid-ion	AMOEBA	Experiment	Theory[a]
$\Delta G_{hydration}$ (kJ/mol)	-1252	-1314	-1315[b]/-1324[c]	-1312
D^{∞} (10^{-5} cm^2/s)	1.2	0.71	0.8[d]/0.955[e]	1.0

[a]Ref. 20, [b]Ref. 54, [c]Ref. 53, [d]Ref. 65, [e]Ref. 66

good accord with the AIMD RDFs and 3D density maps, proved unsuccessful. Moreover, given the complexity of the carbonate/bicarbonate/carbonic acid speciation problem it is possible that the carbonate hydration free energies reported by Marcus may not be directly comparable to results from unreactive simulations with only one CO_3^{2-} ion in the box, which effectively are at infinite dilution where it is not possible to define their pH. Therefore, we decided to prioritize having good agreement with the AIMD and AMOEBA calculations for the structure of the carbonate first hydration shell, a choice that we think is justified by the significant improvement in the $MgCO_3$ ion association constant, as will be shown later in the results section. Overall, the present parameterizations for the polarizable and rigid-ion models performed similarly to or better than the Raiteri et al.[20] rigid-ion force field in describing the thermodynamic and structural properties of hydrated Mg^{2+} and CO_3^{2-} ions.

Mg^{2+}-CO_3^{2-} ion pairing free energy

A known weakness of rigid-ion force field of Raiteri et al.[20] is its inability to correctly reproduce the experimental $Mg-CO_3$ ion pairing free energy. While good agreement was obtained in comparison to the experimental estimates of the pairing free energies for other divalent cations (Ca^{2+}, Sr^{2+}, Ba^{2+}), this force field overestimated the $Mg-CO_3$ association free energy by more than 10 kJ/mol (Table 4), which was largely due to the excessive stability of the contact ion pair state. In fact, a significant difference in the ion pairing

Table 4: Pairing free energies and dissociation constants for the $Mg-CO_3$ ion pair.

	Rigid-ion	AMOEBA	Experiment[a]	Raiteri et al.[b]
ΔG_{IP}	−19.0	−15.4	−17.2	−30.4
pK_{diss}	−3.3	−2.7	−3.0	−5.3

[a]Ref. 20, [b]Ref.[67]

free energy profile obtained with the force fields developed here is the relative stability of the contact and solvent-shared ion pair (SSHIP) states (Figure 3). Compared to the older rigid-ion force field by Raiteri et al.,[20] which predicted the monodentate ion pair to be more stable than the solvent-shared configuration by ≈15 kJ/mol, the reverse was obtained here with both the polarizable AMOEBA and new rigid-ion force fields, which find the SSHIP state at $d_{Mg-C} \approx 4.5$ Å to be the most stable state by 15 and 9 kJ/mol, respectively. A direct consequence of the large destabilization of the CIP relative to the SSHIP state was to significantly decrease the strength of the ion pairing formation free energy (-15 kJ/mol and -19 kJ/mol for AMOEBA and the new rigid-ion model, respectively) compared to the old rigid-ion force field (-30.4 kJ/mol) which brings the current values much closer to the experimental value (-17.2 kJ/mol) from De Visscher et al.,[67] and indeed to bracket it (Table 4).

Significant differences remain between the two models developed in this work, which become apparent only by looking at the 2D free energy maps and the minimum free energy path for ion association as described by the two CVs chosen here (Figure 4). As mentioned previously, the heights of the free energy barriers were largely underestimated in the 1D projection of the free energy (See Figure S7 in the SI). In contrast to other divalent alkaline earth cations, 6-fold coordination by water is expected to be the only readily accessible hydration state for Mg^{2+}; therefore, the formation of the $Mg-CO_3$ ion pair requires the loss of one water molecule from the first Mg^{2+} hydration shell, leading to a high energy barrier of ≈39 kJ/mol and ≈ 51 kJ/mol for the AMOEBA and the new rigid-ion force fields, respectively. Despite the reversed stability order of the CIP and SSHIP states obtained using the former rigid-ion force field, this model also showed a significant free energy barrier (≈27

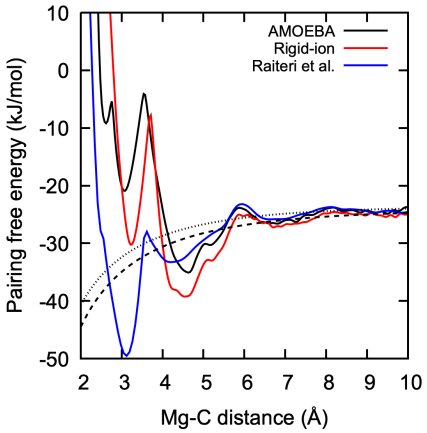

Figure 3: 1D pairing free energies for the $Mg-CO_3$ ion pair formation as a function of the Mg-C distance obtained from the metadynamics simulations after the coordination number collective variable was integrated out using Eq. 4. The dashed lines represent the analytic solutions for the pairing free energy between two point charges interacting via a screened electrostatic potential based on the dielectric constant for the relevant water model.

kJ/mol),[20] though it is lower than for the current models, which is consistent with the less exergonic Mg^{2+} hydration free energy of that force field (Table 2).

Another interesting feature that is noticeable in the 2D free energy map obtained from the AMOEBA force field is the appearance of a shallow intermediate state at $d_{Mg-C} \approx 4.5$ Å where the water coordination number by Mg is five, but the carbonate is still at the SSHIP distance. This intermediate state (IS) could not be observed in the projected 1D profile along the Mg-C distance due to the overlap with the SSHIP minimum along the distance CV. Reaching this five-fold coordinated Mg^{2+} configuration from the SSHIP state is an activated process that requires a high energy barrier (33.6 kJ/mol) to be overcome and its stability is of the order of $2k_BT$ with only a 5.5 kJ/mol barrier to return to the SSHIP minimum. From this intermediate state a further 11.5 kJ/mol is then needed to form the monodentate ion pair, which leads to an overall free energy barrier of ≈39 kJ/mol to be overcome to go from the SSHIP to the CIP. Magnesium carbonate ion pairing would thus appear to be a two-step process with one water molecule leaving the Mg^{2+} hydration shell first, and then CO_3^{2-} moving in closer to form the CIP. This is at variance with the prediction from the

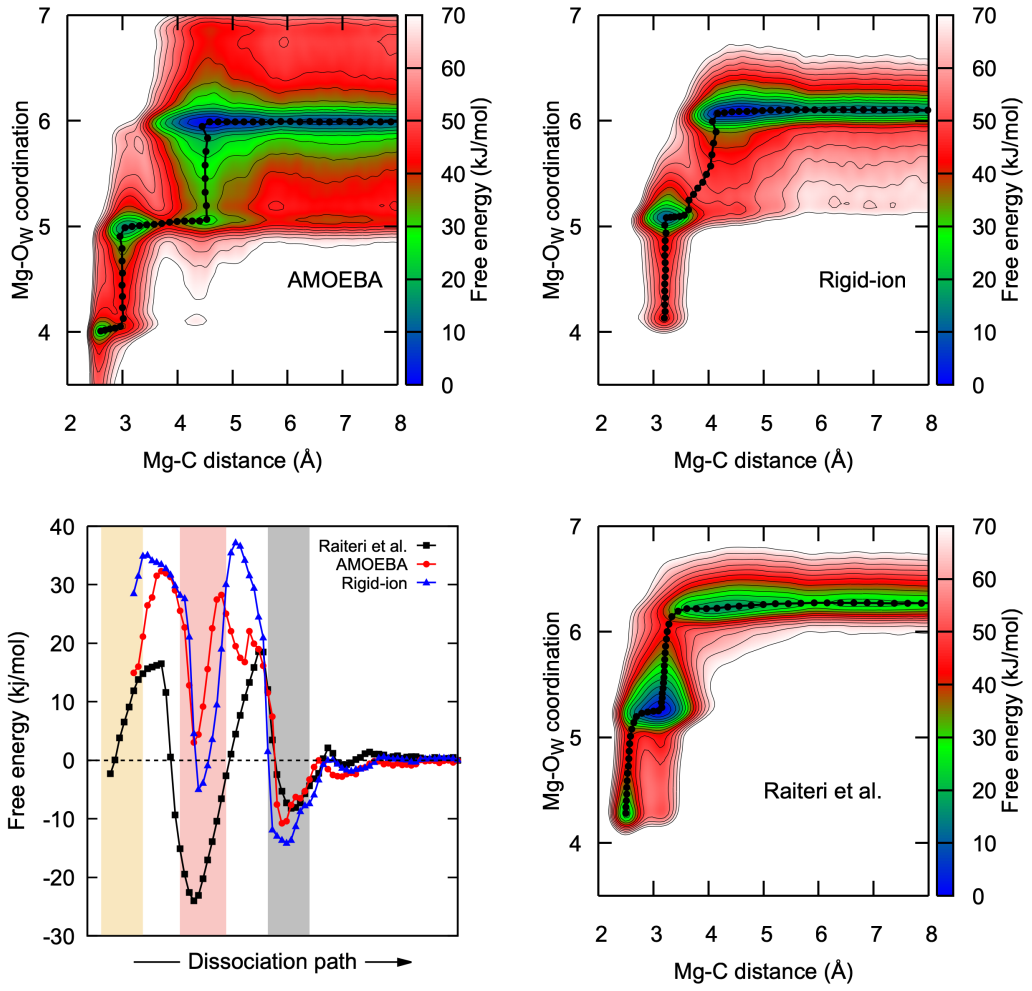

Figure 4: 2D pairing free energies for Mg−CO_3 ion pair formation as a function of the Mg-C distance and the water coordination number by Mg. The minimum free energy path for the dissociation of the Mg−CO_3 ion pair is shown as black beads on the 2D map and as a 1D profile in a separate plot. The shaded yellow, red and gray regions approximately correspond to the bidentate ion pair, monodentate ion pair and solvent shared ion pair, respectively.

old rigid-ion force field, which did not display such minimum in the 2D FES, and whose minimum energy path seems to suggest that the formation of the ion pair would occur with the carbonate group moving closer to Mg^{2+} first and then pushing away one water molecule from the coordination shell. Results obtained with the new parameterization of the rigid-ion force field are more ambiguous and the minimum free energy path seems to suggest a one step process with a concerted movement of the carbonate entering the magnesium inner shell while a water molecule simultaneously leaves.

In the case of the AMOEBA-based simulation, another important piece of information given by the 2D FES compared to the 1D projection pertains to the stability and free energy barrier associated with the monodentate to bidentate transition for the CIP. As discussed before, the 1D projection along the Mg-C distance leads to an underestimation of this barrier due to an overlap of the bidentate and monodentate free energy basins along the water coordination number by Mg. The minimum energy path from the 2D FES reveals that the monodentate to bidentate transition requires twice as much energy (29.5 kJ/mol) as the 1D projection would suggest (15.1 kJ/mol). While the reverse process appears almost barrierless in one-dimension (3.8 kJ/mol), there is in fact a higher 17.5 kJ/mol barrier to return to the monodentate configuration. In both cases, the relative stabilities of the two states remain the same, with the monodentate ion pair more stable by about ≈12 kJ/mol. At variance with the AMOEBA force field, the rigid-ion model predicts the bidentate CIP to be only a shallow free energy minimum and much higher in free energy (+33 kJ/mol) than the CIP state.

In order to further probe the bidentate-monodentate transition we also carried out an *ab initio* molecular dynamics simulation with well-tempered metadynamics. The 2D map of the free energy for $MgCO_3$ as a function of the two biased CVs, the water and carbonate coordination numbers by Mg obtained from AIMD simulations, is shown in Figure 5. We also note that the calculated water coordination numbers were overestimated by about 0.5 compared to the expected ones due to the extended range of the switching function.

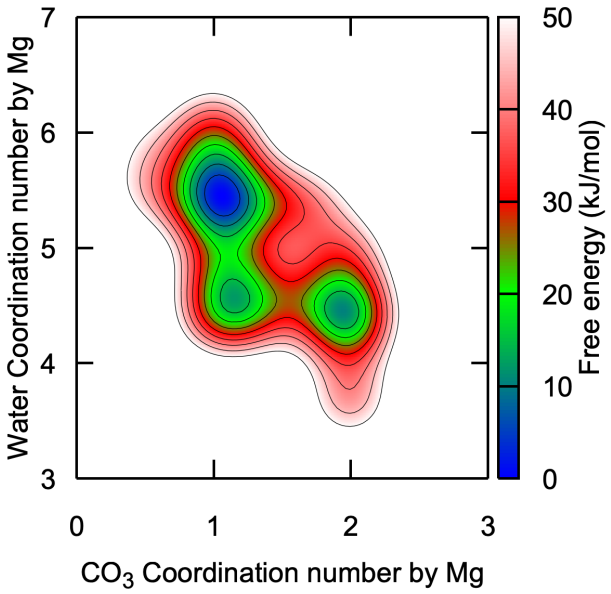

Figure 5: AIMD free energy for $MgCO_3$ as a function of the water and carbonate coordination numbers by Mg (biased CVs), showing the monodentate and bidentate states of the contact ion pair.

Three free energy minima were obtained, corresponding to the bidentate state, a monodentate state in which Mg is only five-fold coordinated, and the expected monodentate state with a six-fold coordinated cation, in order of increasing stability. The monodentate state was found to be more stable than the bidentate configuration by about 15 kJ/mol which is in good agreement with the AMOEBA results. The transition from the monodentate to the bidentate state involved overcoming two consecutive ≈20 kJ/mol barriers for one water molecule to leave the Mg^{2+} hydration shell first, and finally for the carbonate to bind in a bidentate configuration. It is thus not surprising that the simulation carried out with the AMOEBA force field, which did not show a minimum for the five-fold Mg^{2+} monodentate state (i.e. CNw=4, CNcarb=1), predicted a free energy barrier falling halfway between 20 and 40 kJ/mol. Although no minimum was found for this configuration with the polarizable force field, the minimum free energy path on the 2D FES would suggest that, similarly to the SSHIP-to-monodentate transition, the formation of the bidentate CIP first involves a decrease of the water coordination number by Mg while the Mg-C distance remains unchanged,

and then a shortening of the Mg-C distance, i.e. bidentate binding, in agreement with the *ab initio* results. Here, poorer agreement is obtained with the new rigid-ion model, which predicts the free energy difference between monodentate and bidentate states, ≈33 kJ/mol, to be more than double the *ab initio* (≈15 kJ/mol) and AMOEBA (≈12 kJ/mol) values.

Compared to the previous force field, the present parameterizations for the rigid-ion and polarizable models of Mg^{2+} and CO_3^{2-} in water represent a substantial improvement in reproducing both the experimental and AIMD data on magnesium carbonate ion pairing. The only significant shortcoming of the new rigid-ion force field is to over-destabilize the bidentate ion pair compared to the monodentate state. Hence, in the next section we will discuss water exchange around Mg^{2+} only for this new rigid-ion force field.

Water exchange

Water exchange around the Mg^{2+} ion was studied using metadynamics simulations with the two collective variables being the distance between Mg^{2+} and a selected water molecule (d_{Mg-O_w}) and the Mg^{2+} coordination number with respect to all the remaining water molecules (Figure 6). This choice of CVs was inspired by the work of Schwierz[3] where the water exchange around the Mg ion was found to involve the concerted movement of all the water molecules in the Mg^{2+} solvation shell to produce a symmetric transition state. Although the coordination number does not impose any symmetry on the structure of the hydration shell, it introduces a bias potential on the coordination shell that is orthogonal to the distance collective variable and allows for a more accurate description of the water exchange barrier.

It is worth mentioning here that the choice of making one water molecule effectively distinguishable from the others, has important consequences on the resulting Mg–water pairing free energy. Despite the fact that the system's total free energy is independent of which water molecule coordinates the Mg^{2+} ion, the free energy projected on the distance between the ion and a specific water molecule need not be the same when the molecule is in contact with the ion or not. In fact, the free energy as a function of the distance

between the Mg^{2+} ion and the tagged water molecule has the same limiting behavior as the $Mg-CO_3$ ion pairing free energy, i.e. it asymptotically diverges to $-\infty$ with increasing distance, as discussed in the Supporting Information (See Figure XX in the SI). The 2D free

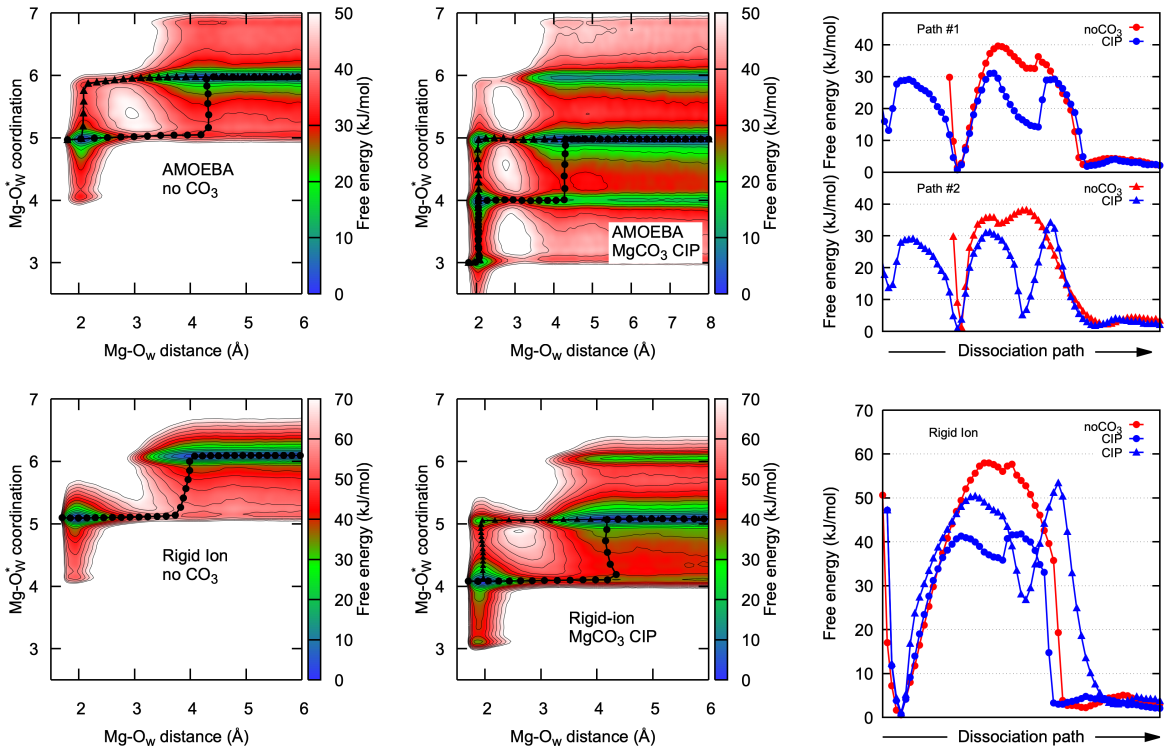

Figure 6: 2D free energy maps as a function of the distance between Mg and a selected water molecule and of the Mg coordination number with respect to all other water molecules (see text for details). The results for the AMOEBA and rigid-ion force fields are reported in the top and bottom lines, respectively, while the 2D maps on the left and center are for the Mg^{2+} alone and when in a contact ion pair with carbonate, also respectively. The beads on the free energy maps correspond to the minimum free energy paths (shown in the right-hand column) for the dissociative (circles) and associative (triangles) water exchange mechanisms.

energy surface computed in the absence of carbonate has the expected behaviour, i.e. Mg^{2+} is always 6-fold coordinated, if we account for the fact that the total magnesium by water coordination number increases by one when the tagged water molecule is within 3 Å of the ion. While the rigid-ion force field predicts that the water exchange occurs via a dissociative mechanism, the AMOEBA model shows that both the associative and dissociative paths are competitive. The free energy barriers computed from the minimum free energy paths (Figure 6 using the AMOEBA force field (≈37 kJ/mol) are in good agreement with the

experimental estimates (39.8[67] and 40.2[68]), while the rigid-ion force field overestimates the free energy of the transition state by almost 20 kJ/mol (Table 5).

The water exchange mechanisms become more complicated when Mg is in a contact ion pair with carbonate where multiple exchange pathways are now possible, particularly for the AMOEBA model. However, the dissociative (path #1) and associative (path #2) are still the dominant ones. Interestingly, the free energy barrier for the dissociative mechanism is significantly reduced by the presence of the carbonate ion (Table 5), while the barrier for the associative mechanism appears to be less affected by the presence of carbonate. Both the AMOEBA and rigid-ion model predict a reduction of the free energy barrier of about 20-30%, which suggests that the water exchange rate around would be significantly faster when the Mg^{2+} is in an ion pair with carbonate.

Table 5: Free energy barrier heights for water exchange around free Mg^{2+} and Mg^{2+} bound to carbonate as part of a contact ion pair (kJ/mol). The values were obtained from the minimum energy path computed on the 2D metadynamics simulations where the carbonate was absent or restrained to be in the first coordination shell of Mg^{2+}.

	Rigid-ion	AMOEBA	Experiment
$Mg-H_2O$	59.4	37.0	$39.8^a/40.2^b$
$MgCO_3-H_2O$	41.3	28.5	
$\Delta\Delta G$	-18.1	-8.5	

[a]Ref. 67, [b]Ref. 68

Accuracy of the calculations

Because there is no formula to estimate the accuracy of the metadynamics calculations, a careful choice of the simulation parameters and repetition of the calculations using different configurations are the only tools at our disposal to ensure the reliability of the free energy calculations. In particular, the use of the well-tempered and multiple-walkers methods to progressively reduce the barrier height and to parallelize the free energy calculations[43,45] provide us some guidance as to the reliability of the calculations. Although we can assume that the metadynamics calculation has converged when the height of the added Gaussians

drops significantly below thermal energy ($< 0.01 k_B T$) throughout the relevant parts of the free energy space that we want to explore, this alone is not sufficient to guarantee that the relative stability of the free energy minima and barrier heights have been accurately calculated. In fact the well-tempered method does not flatten out the free energy surface, but it reduces the barrier heights by the magnitude of the bias factor chosen, *e.g* a bias factor of 20 would reduce a free energy barrier of 60 kJ/mol to 3 kJ/mol, which can be easily overcome by thermal fluctuations (Figures S13 and S14 in the SI). Hence, a bias factor that is too small does not allow for an accurate estimate of the free energy barrier, while using a value that is too large would waste computational resources by making the simulation very slow to converge. Without knowing *a priori* what the largest free energy barrier in the system actually is, we can only assess whether the chosen bias factor is appropriate for the simulation in post-processing by monitoring the behaviour of the multiple walkers and making sure that all the free energy barriers are regularly crossed, particularly toward the end of the simulations. In fact, by starting each walker from different positions within the region of interest, we effectively predetermine how the space will be explored and if the walkers are not able to cross the free energy barriers, this not only limits our accuracy as to the estimate of the free energy barriers but it also biases the relative stability of the free energy minima. Therefore, it is good practice to repeat any well-tempered and multiple-walker simulations by using different bias factors and initial distributions of the walkers. Non-reproducible free energy surfaces are a clear indication that either an important (slow) collective variable has been missed or that the well-tempered parameters were not appropriate for the system at hand.

Due to the lower computational cost of the rigid-ion force field we have repeated all the metadynamics calculations three times with different starting configurations, two different choices of the switching function parameters and and three different values for the bias factor (10, 20 and 30), which gave quantitatively similar barrier heights (Figures S9−S14 in the Supporting Information). To further probe the effect of the restraining potential we

also performed a further metadynamics simulation using the Mg−CO_3 distance as a third collective variable (Figure 7). Due to the significantly larger size of the free energy space to be explored, we increased the width of the Gaussians to 0.2, in the CV units, and we ran the well-tempered multiple-walker metadynamics simulations for 1 μs with a bias factor of 20. We then extracted the minimum energy path for water exchange at different values of the Mg−CO_3 distance, which gave free energy barriers consistent with the results shown above. Finally, we also tested the effect of the switching function used in the rigid-ion calculations

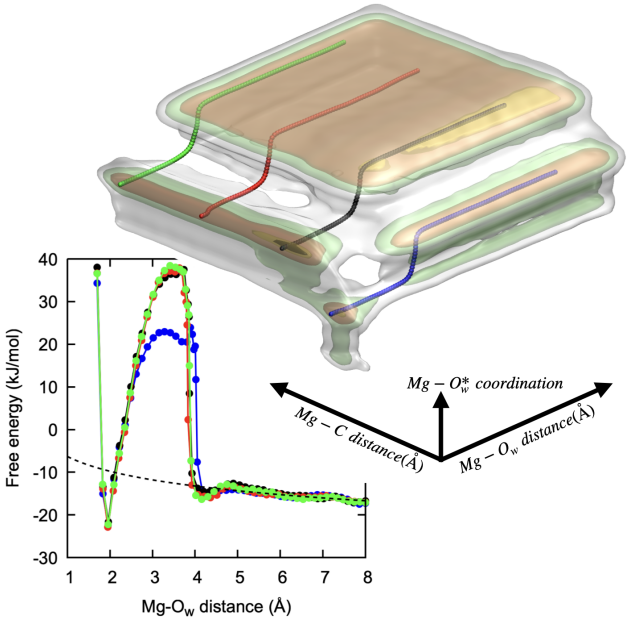

Figure 7: Three dimensional free energy surface as a function of the distances between Mg and one water molecules and the carbon atom in carbonate, and of the coordination number between Mg and the remaining water molecules computed with the rigid-ion force field. The isosurfaces correspond to free energies of 5, 10, 30, 50 and 70 kJ/mol relative to the global minimum and are colored in black, yellow, red, green and white, respectively. The colored beads correspond to the minimum free energy path for water exchange at different Mg−CO_3 distances, 3.2, 5 and 7 Å, which correspond to the CIP, SSHIP and separated states, respectively. The free energy along these paths is also shown as a 1D projection in the graph with corresponding colors.

by further repeating the metadynamics calculations with 2 and 3 CVs; again the results showed consistent free energy barriers and are reported in the Supporting Information.

Although we cannot absolutely prove that our choice of CVs provides a correct description of the true reaction coordinate, every metadynamics simulation that we have run where the

coordination number CV was included provided quantitatively consistent results for the stability of the various states and for the transition barrier heights, unlike the case where only the distance between Mg one (or two) water molecules were used (Figure S16 and S17 in the Supporting Information). Moreover, in the case of of the water exchange of an isolated Mg ion we have performed a committor analysis, which shows that frames selected from around the maximum of the free energy barrier obtained on the minimum energy path have an almost equal probability of going forward or backwards, as expected for the true transition state (Figure S18 in the Supporting Information). Overall, we believe that the free energies reported here have an accuracy comparable to k_BT, with the caveat that the free energy barriers are a lower bound to the exact barrier on the real reaction coordinate. Due to the computational cost of the polarizable AMOEBA force field we could not perform such an extensive set of validation calculations but given the agreement between the results shown here we would expect a similar degree of accuracy.

Assessing the accuracy of the free energy calculations obtained from AIMD is much more difficult. Although any statistical error is expected to be much larger than for the rigid-ion simulations, we have employed strategies to try minimize the influence of this factor. Importantly, we have limited as much as possible the size of the space to be explored during the AIMD and have used two walkers, which should slightly reduce the bias due to the choice of the starting configuration. In addition, by studying only the transition between the mono- and bi-dentate configuration we have limited the errors related to charge localization on the anion, which has been shown to be a problem for the determination of the ion pair binding free energy from DFT,[26] as is the necessary use of a smaller cell size. For further information regarding the error analysis relating to the AIMD see Figures S5 and S6 and associated text in the Supporting Information.

Conclusions

The present parameterizations of both the polarizable and rigid-ion models reproduce accurately the hydration structures of magnesium and carbonate in aqueous solution. Importantly, the magnesium carbonate ion pairing free energies are now in excellent agreement with experimental data, which is a significant improvement over former rigid-ion models.[20] However, unlike the rigid-ion model, the polarizable force field is also able to reproduce the *ab initio* free energy difference between the bidentate and monodentate states of the contact ion pair. Although the polarizable AMOEBA force field appears to be superior to the rigid-ion one, the latter would still provide a qualitatively accurate description of the thermodynamics of the aqueous $Mg-CO_3$ system. Due to its lower computational cost, this rigid-ion force field could therefore be more readily used to explore $Mg/CaCO_3$ nucleation and growth processes where long simulations with large systems need to be used.

The accurate description of Mg^{2+}-CO_3^{2-} ion pair formation is key in describing the water exchange around Mg^{2+} in the presence of carbonate. Metadynamics simulations conducted with both force fields find that the formation of a contact magnesium carbonate ion pair decreases the energy barrier for water exchange relative to free Mg^{2+} in solution. Similar behaviour has been reported for other metal ion-ligand complexes,[69,70] but to the best of our knowledge no experimental values are available for water exchange around the $Mg-CO_3$ complex. Our prediction that water exchange is more labile around the $Mg-CO_3$ complex is at variance with the computational results from Yang et al.[27] and Hamm et al.,[28] who did not observe any significant increase in the water exchange rate when Mg^{2+} formed a complex with either HS^- or aspartate. However, Lincoln[69] suggested that each metal ion-ligand complex behaves differently; for example he reported that CrO_4^{2-} increases the water lability of the aqueous Ca^{2+} ion but has little effect on the water exchange around Mg^{2+}, therefore more experimental work on the magnesium carbonate system is required to corroborate our results.

The above result is significant as it suggests that the presence of carbonate can ac-

celerate water exchange around the aqueous Mg^{2+} ion, which is generally regarded as the rate-limiting step for the nucleation of magnesium-bearing minerals. The presence of ion pairs could also play a significant role in a wide range of geochemical phenomena such as ion adsorption, nucleation and biomineralization, and this result could have significant implications in biochemistry where the transport of Mg^{2+} ions across cell membranes and their catalytic activity help regulate many physiological processes in living organisms.

In this work we have also provided a thorough validation of the computational methodology used to compute the free energy barrier for the water exchange around aqueous ions. We have demonstrated how in the case of Mg^{2+} two collective variables are required to describe the water exchange mechanism, which is in agreement with a previous study by Schwierz[3] that suggests that this process requires the concerted motion of all the water molecules in the ion's hydration shell. The accurate calculation of water exchange rates around aqueous ions is not a trivial task, even having determined the free energy barrier, since transition state theory may not provide a reliable estimate without correction for recrossing events. Based on the reduction in barrier heights due to ion pairing, the relative increase in rates can be estimated to be between 2 and 3 orders of magnitude. However, the full computation of absolute rate constants remains a task for future work.

Acknowledgement

The Australian Research Council is acknowledged for funding under grant FL180100087, as well as the Pawsey Supercomputing Centre and National Computational Infrastructure for provision of computational resources.

Supporting Information Available

Derivation of all the equations used to compute the ion association constant from enhanced sampling simulations. Numerical validation of those equations. Discussion about the con-

vergence of the calculations. Effect of changing the switching function and bias factor in the metadynamics calculations.

References

(1) Woodson, S. A. Metal ions and RNA folding: a highly charged topic with a dynamic future. *Curr. Opin. Chem. Biol.* **2005**, *9*, 104–109.

(2) Ko, Y. H.; Hong, S.; Pedersen, P. L. Chemical mechanism of ATP synthase. *J. Biol. Chem.* **1999**, *274*, 28853–28856.

(3) Schwierz, N. Kinetic pathways of water exchange in the first hydration shell of magnesium. *J. Chem. Phys.* **2020**, *152*, 224106.

(4) Warren, J. Dolomite: occurrence, evolution and economically important associations. *Earth Sci. Rev.* **2000**, *52*, 1–81.

(5) Lindtke, J.; Ziegenbalg, S. B.; Brunner, B.; Rouchy, J. M.; Pierre, C.; Peckmann, J. Authigenesis of native sulphur and dolomite in a lacustrine evaporitic setting (Hellín basin, Late Miocene, SE Spain). *Geol. Mag.* **2011**, *148*, 655–669.

(6) Meister, P.; Reyes, C.; Beaumont, W.; Rincon, M.; Collins, L.; Berelson, W.; Stott, L.; Corsetti, F.; Nealson, K. H. Calcium and magnesium-limited dolomite precipitation at Deep Springs Lake, California. *Sedimentology* **2011**, *58*, 1810–1830.

(7) Van Tuyl, F. M. The origin of dolomite. *Iowa Geol. Surv. Annu. Rep.* **1916**, *25*, 251–422.

(8) Chang, B. et al. Massive formation of early diagenetic dolomite in the Ediacaran ocean: Constraints on the "dolomite problem". *Proc. Natl. Acad. Sci. U. S. A.* **2020**, *117*, 14005–14014.

(9) Rodriguez-Blanco, J. D.; Shaw, S.; Benning, L. G. A route for the direct crystallization of dolomite. *Am. Mineral.* **2015**, *100*, 1172–1181.

(10) Lippmann, F. *Sedimentary carbonate minerals*, 1973rd ed.; Minerals and Rocks; Springer: Berlin, Germany, 1973.

(11) Graf, D. L.; Goldsmith, J. R. Some hydrothermal syntheses of dolomite and protodolomite. *J. Geol.* **1956**, *64*, 173–186.

(12) Kaczmarek, S. E.; Sibley, D. F. Direct physical evidence of dolomite recrystallization. *Sedimentology* **2014**, *61*, 1862–1882.

(13) Gregg, J. M.; Bish, D. L.; Kaczmarek, S. E.; Machel, H. G. Mineralogy, nucleation and growth of dolomite in the laboratory and sedimentary environment: A review. *Sedimentology* **2015**, *62*, 1749–1769.

(14) Kell-Duivestein, I. J.; Baldermann, A.; Mavromatis, V.; Dietzel, M. Controls of temperature, alkalinity and calcium carbonate reactant on the evolution of dolomite and magnesite stoichiometry and dolomite cation ordering degree - An experimental approach. *Chem. Geol.* **2019**, *529*, 119292.

(15) Pina, C. M.; Pimentel, C.; Crespo, Á. Dolomite cation order in the geological record. *Chem. Geol.* **2020**, *547*, 119667.

(16) Vasconcelos, C.; McKenzie, J. A.; Bernasconi, S.; Grujic, D.; Tiens, A. J. Microbial mediation as a possible mechanism for natural dolomite formation at low temperatures. *Nature* **1995**, *377*, 220–222.

(17) Qiu, X.; Wang, H.; Yao, Y.; Duan, Y. High salinity facilitates dolomite precipitation mediated by Haloferax volcanii DS52. *Earth Planet. Sci. Lett.* **2017**, *472*, 197–205.

(18) Kaczmarek, S. E.; Gregg, J. M.; Bish, D. L.; Machel, H. G.; Fouke, B. W. *Characterization and Modeling of Carbonates–Mountjoy Symposium 1*; SEPM (Society for Sedimentary Geology), 2017; pp 7–20.

(19) Bleuzen, A.; Pittet, P.-A.; Helm, L.; Merbach, A. E. Water exchange on magnesium(II) in aqueous solution: a variable temperature and pressure 17O NMR study. *Magnetic Resonance in Chemistry* **1997**, *35*, 765–773.

(20) Raiteri, P.; Demichelis, R.; Gale, J. D. Thermodynamically consistent force field for molecular dynamics simulations of alkaline-earth carbonates and their aqueous speciation. *J. Phys. Chem. C* **2015**, *119*, 24447–24458.

(21) Grotz, K. K.; Cruz-León, S.; Schwierz, N. Optimized magnesium force field parameters for biomolecular simulations with accurate solvation, ion-binding, and water-exchange properties. *J. Chem. Theory Comput.* **2021**, *17*, 2530–2540.

(22) Soniat, M.; Hartman, L.; Rick, S. W. Charge transfer models of zinc and magnesium in water. *J. Chem. Theory Comput.* **2015**, *11*, 1658–1667.

(23) Martinek, T.; Duboué-Dijon, E.; Timr, Š.; Mason, P. E.; Baxová, K.; Fischer, H. E.; Schmidt, B.; Pluhařová, E.; Jungwirth, P. Calcium ions in aqueous solutions: Accurate force field description aided by ab initio molecular dynamics and neutron scattering. *J. Chem. Phys.* **2018**, *148*, 222813.

(24) Duboué-Dijon, E.; Mason, P. E.; Fischer, H. E.; Jungwirth, P. Hydration and ion pairing in aqueous Mg2+ and Zn2+ solutions: Force-field description aided by neutron scattering experiments and ab initio molecular dynamics simulations. *J. Phys. Chem. B* **2018**, *122*, 3296–3306.

(25) Ponder, J. W.; Wu, C.; Ren, P.; Pande, V. S.; Chodera, J. D.; Schnieders, M. J.; Haque, I.; Mobley, D. L.; Lambrecht, D. S.; DiStasio, R. A., Jr; Head-Gordon, M.; Clark, G. N. I.; Johnson, M. E.; Head-Gordon, T. Current status of the AMOEBA polarizable force field. *J. Phys. Chem. B* **2010**, *114*, 2549–2564.

(26) Raiteri, P.; Schuitemaker, A.; Gale, J. D. Ion pairing and multiple ion binding in calcium carbonate solutions based on a polarizable AMOEBA force field and ab initio molecular dynamics. *J. Phys. Chem. B* **2020**, *124*, 3568–3582.

(27) Yang, Y.; Sahai, N.; Romanek, C. S.; Chakraborty, S. A computational study of Mg2+

dehydration in aqueous solution in the presence of HS- and other monovalent anions – Insights to dolomite formation. *Geochim. Cosmochim. Acta* **2012**, *88*, 77–87.

(28) Hamm, L. M.; Wallace, A. F.; Dove, P. M. Molecular dynamics of ion hydration in the presence of small carboxylated molecules and implications for calcification. *J. Phys. Chem. B* **2010**, *114*, 10488–10495.

(29) Mendes de Oliveira, D.; Zukowski, S. R.; Palivec, V.; Hénin, J.; Martinez-Seara, H.; Ben-Amotz, D.; Jungwirth, P.; Duboué-Dijon, E. Binding of divalent cations to acetate: molecular simulations guided by Raman spectroscopy. *Phys. Chem. Chem. Phys.* **2020**, *22*, 24014–24027.

(30) Eastman, P.; Swails, J.; Chodera, J. D.; McGibbon, R. T.; Zhao, Y.; Beauchamp, K. A.; Wang, L.-P.; Simmonett, A. C.; Harrigan, M. P.; Stern, C. D.; Wiewiora, R. P.; Brooks, B. R.; Pande, V. S. OpenMM 7: Rapid development of high performance algorithms for molecular dynamics. *PLoS Comput. Biol.* **2017**, *13*, e1005659.

(31) Friedrichs, M. S.; Eastman, P.; Vaidyanathan, V.; Houston, M.; Legrand, S.; Beberg, A. L.; Ensign, D. L.; Bruns, C. M.; Pande, V. S. Accelerating molecular dynamic simulation on graphics processing units. *J. Comput. Chem.* **2009**, *30*, 864–872.

(32) Eastman, P.; Pande, V. S. Efficient nonbonded interactions for molecular dynamics on a graphics processing unit. *J. Comput. Chem.* **2010**, *31*, 1268–1272.

(33) Wu, Y.; Tepper, H. L.; Voth, G. A. Flexible simple point-charge water model with improved liquid-state properties. *J. Chem. Phys.* **2006**, *124*, 024503.

(34) Thompson, A. P.; Aktulga, H. M.; Berger, R.; Bolintineanu, D. S.; Brown, W. M.; Crozier, P. S.; in 't Veld, P. J.; Kohlmeyer, A.; Moore, S. G.; Nguyen, T. D.; Shan, R.; Stevens, M. J.; Tranchida, J.; Trott, C.; Plimpton, S. J. LAMMPS - a flexible simulation tool for particle-based materials modeling at the atomic, meso, and continuum scales. *Comput. Phys. Commun.* **2022**, *271*, 108171.

(35) PLUMED consortium, Promoting transparency and reproducibility in enhanced molecular simulations. *Nat. Methods* **2019**, *16*, 670–673.

(36) Tribello, G. A.; Bonomi, M.; Branduardi, D.; Camilloni, C.; Bussi, G. PLUMED 2: New feathers for an old bird. *Comput. Phys. Commun.* **2014**, *185*, 604–613.

(37) Laury, M. L.; Wang, L.-P.; Pande, V. S.; Head-Gordon, T.; Ponder, J. W. Revised parameters for the AMOEBA polarizable atomic multipole water model. *J. Phys. Chem. B* **2015**, *119*, 9423–9437.

(38) Marcus, Y. *Ions in Solution and their Solvation*; John Wiley & Sons: Nashville, TN, 2015.

(39) Kirkwood, J. G. Statistical mechanics of fluid mixtures. *J. Chem. Phys.* **1935**, *3*, 300–313.

(40) Bennett, C. H. Efficient estimation of free energy differences from Monte Carlo data. *J. Comput. Phys.* **1976**, *22*, 245–268.

(41) Lagardère, L.; Jolly, L.-H.; Lipparini, F.; Aviat, F.; Stamm, B.; Jing, Z. F.; Harger, M.; Torabifard, H.; Cisneros, G. A.; Schnieders, M. J.; Gresh, N.; Maday, Y.; Ren, P. Y.; Ponder, J. W.; Piquemal, J.-P. Tinker-HP: a massively parallel molecular dynamics package for multiscale simulations of large complex systems with advanced point dipole polarizable force fields. *Chem. Sci.* **2018**, *9*, 956–972.

(42) Gale, J. D.; Rohl, A. L. The general utility lattice program (GULP). *Mol. Simul.* **2003**, *29*, 291–341.

(43) Bussi, G.; Donadio, D.; Parrinello, M. Canonical Sampling Through Velocity Rescaling. *Journal of Chemical Physics* **2007**, *126*, 014101.

(44) Barducci, A.; Bussi, G.; Parrinello, M. Well-tempered metadynamics: a smoothly converging and tunable free-energy method. *Phys. Rev. Lett.* **2008**, *100*, 020603.

(45) Raiteri, P.; Laio, A.; Gervasio, F. L.; Micheletti, C.; Parrinello, M. Efficient reconstruction of complex free energy landscapes by multiple walkers metadynamics. *J. Phys. Chem. B* **2006**, *110*, 3533–3539.

(46) Laio, A.; Parrinello, M. Escaping free-energy minima. *Proc. Natl. Acad. Sci. U. S. A.* **2002**, *99*, 12562–12566.

(47) Byrne, E. H.; Raiteri, P.; Gale, J. D. Computational Insight into Calcium-Sulfate Ion Pair Formation. *Journal of Physical Chemistry C* **2017**, *121*, 25956–25966.

(48) Fuoss, R. M.; Kraus, C. A. Properties of electrolytic solutions. III. The dissociation constant. *Journal of The American Chemical Society* **1933**, *55*, 1019–1028.

(49) VandeVondele, J.; Krack, M.; Mohamed, F.; Parrinello, M.; Chassaing, T.; Hutter, J. Quickstep: Fast and accurate density functional calculations using a mixed Gaussian and plane waves approach. *Comput. Phys. Commun.* **2005**, *167*, 103–128.

(50) Hutter, J.; Iannuzzi, M.; Schiffmann, F.; VandeVondele, J. cp2k: atomistic simulations of condensed matter systems. *Wiley Interdiscip. Rev. Comput. Mol. Sci.* **2014**, *4*, 15–25.

(51) Bankura, A.; Karmakar, A.; Carnevale, V.; Chandra, A.; Klein, M. L. Structure, dynamics, and spectral diffusion of water from first-principles molecular dynamics. *J. Phys. Chem. C* **2014**, *118*, 29401–29411.

(52) Ohtaki, H.; Radnai, T. Structure and dynamics of hydrated ions. *Chem. Rev.* **1993**, *93*, 1157–1204.

(53) Marcus, Y. Thermodynamics of solvation of ions. Part 5.—Gibbs free energy of hydration at 298.15 K. *J. Chem. Soc., Faraday Trans.* **1991**, *87*, 2995–2999.

(54) Marcus, Y. A simple empirical model describing the thermodynamics of hydration of ions of widely varying charges, sizes, and shapes. *Biophys. Chem.* **1994**, *51*, 111–127.

(55) David, F.; Vokhmin, V.; Ionova, G. Water characteristics depend on the ionic environment. Thermodynamics and modelisation of the aquo ions. *J. Mol. Liq.* **2001**, *90*, 45–62.

(56) Schmid, R.; Miah, A. M.; Sapunov, V. N. A new table of the thermodynamic quantities of ionic hydration: values and some applications (enthalpy–entropy compensation and Born radii). *Phys. Chem. Chem. Phys.* **2000**, *2*, 97–102.

(57) Noyes, R. M. Thermodynamics of ion hydration as a measure of effective dielectric properties of water. *J. Am. Chem. Soc.* **1962**, *84*, 513–522.

(58) Rosseinsky, D. R. Electrode potentials and hydration energies. Theories and correlations. *Chem. Rev.* **1965**, *65*, 467–490.

(59) Jiang, Y.; Zhang, H.; Tan, T. Rational design of methodology-independent metal parameters using a nonbonded dummy model. *J. Chem. Theory Comput.* **2016**, *12*, 3250–3260.

(60) Mills, R.; Lobo, V. M. M. *Self-diffusion in electrolyte solutions*; Physical sciences data; Elsevier Science: London, England, 1989.

(61) Tissandier, M. D.; Cowen, K. A.; Feng, W. Y.; Gundlach, E.; Cohen, M. H.; Earhart, A. D.; Coe, J. V.; Tuttle, T. R. The proton's absolute aqueous enthalpy and Gibbs free energy of solvation from cluster-ion solvation data. *J. Phys. Chem. A* **1998**, *102*, 7787–7794.

(62) Gomer, R.; Tryson, G. An experimental determination of absolute half-cell emf's and single ion free energies of solvation. *J. Chem. Phys.* **1977**, *66*, 4413–4424.

(63) Allnér, O.; Nilsson, L.; Villa, A. Magnesium ion-water coordination and exchange in biomolecular simulations. *J. Chem. Theory Comput.* **2012**, *8*, 1493–1502.

(64) Yeh, I.-C.; Hummer, G. System-size dependence of diffusion coefficients and viscosities from molecular dynamics simulations with periodic boundary conditions. *J. Phys. Chem. B* **2004**, *108*, 15873–15879.

(65) Kigoshi, K.; Hashitani, T. The self-diffusion coefficients of carbon dioxide, hydrogen carbonate ions and carbonate ions in aqueous solutions. *Bull. Chem. Soc. Jpn.* **1963**, *36*, 1372–1372.

(66) Yuan-Hui, L.; Gregory, S. Diffusion of ions in sea water and in deep-sea sediments. *Geochim. Cosmochim. Acta* **1974**, *38*, 703–714.

(67) De Visscher, A.; Vanderdeelen, J.; Königsberger, E.; Churagulov, B. R.; Ichikuni, M.; Tsurumi, M. IUPAC-NIST solubility data series. 95. Alkaline earth carbonates in aqueous systems. Part 1. Introduction, be and mg. *J. Phys. Chem. Ref. Data* **2012**, *41*, 013105–67.

(68) Neely, J.; Connick, R. Rate of water exchange from hydrated magnesium ion. *J. Am. Chem. Soc.* **1970**, *92*, 3476–3478.

(69) Lincoln, S. Mechanistic Studies of Metal Aqua Ions: A Semi-Historical Perspective. *Helvetica Chimica Acta* **2005**, *88*, 523–545.

(70) Maigut, J.; Meier, R.; Zahl, A.; Eldik, R. v. Triggering Water Exchange Mechanisms via Chelate Architecture. Shielding of Transition Metal Centers by Aminopolycarboxylate Spectator Ligands. *Journal of the American Chemical Society* **2008**, *130*, 14556–14569.

TOC Graphic